Nanoscale

Accepted Manuscript

This article can be cited before page numbers have been issued, to do this please use: L. Zeng, F. Pan, W. Li, Y. Jiang, X. Zhong and Y. Yu, *Nanoscale*, 2014, DOI: 10.1039/C4NR02498B.

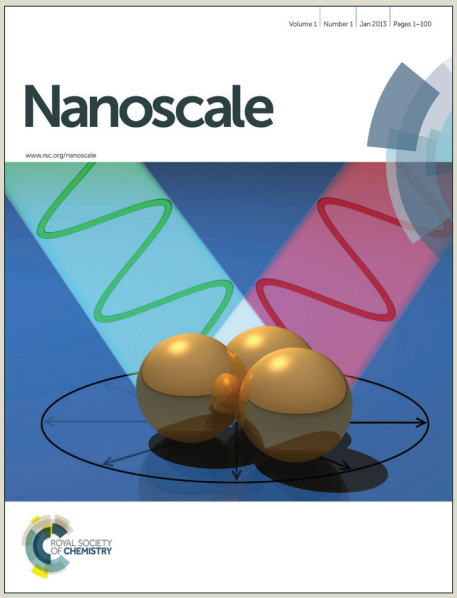

ROYAL SOCIETY OF CHEMISTRY

www.rsc.org/nanoscale

View Article Online
DOI: 10.1039/C4NR02498B

Free-standing Porous Carbon Nanofibers-Sulfur Composite for Flexible Li-S Battery Cathode

Linchao Zeng, Fusen Pan, Weihan Li, Yu Jiang, Xiongwu Zhong, Yan Yu*

CAS Key Laboratory of Materials for Energy Conversion, Department of Materials Science and Engineering, University of Science and Technology of China, Anhui Hefei 230026, China, E-mail:yanyumse@ustc.edu.cn

Abstract

Flexible and free-standing sulphur/(PCNFs-CNT) composite (S@PCNFs-CNT) electrode was successfully prepared by infiltrating sulfur into microporous carbon nanofibers-carbon nanotube (PCNFs-CNT) composite. When used as a cathode material for Li-S batteries, the S@PCNFs-CNT exhibits much better cycle performance and rate performance compare to CNT-free S@PCNFs. It delivers a reversible capacity of 637 $mAhg^{-1}$ after 100 cycles at 50 mAg^{-1} and a rate capability of 437 $mAhg^{-1}$ at 1 Ag^{-1}. The improved electrochemical performance is attributed to synergistic effect of the 3D interconnected structure, the additive of CNT, the uniform distribution of micropores (< 2 nm) in the PCNFs-CNT matrix. Our results indicate the potential suitability of PCNFs-CNT for efficient, free-standing, high-performance batteries.

Keywords: microporous; CNT-doping; morphology stability

1. Introduction

Lithium-ion batteries (LIBs) have been great successful in portable electronics such as laptops, cameras and mobile phones over the last two decades.[1-4] However, present research of cathodes based on intercalate mechanism such as $LiCoO_2$[5], $LiMn_2O_4$[6] and $LiFePO_4$[7] almost approached their theoretical energy density limits and cannot meet the demand in electric vehicles (EV), plug-in hybrid vehicles (HEV)

View Article Online
DOI: 10.1039/C4NR02498B

and grid energy storage.[8-10] To meet the requirements of large-scale energy storage devices, one effective way is to find novel alternative electrochemically active materials with high capacity and new redox concepts.[11-17] Among these cathode materials, sulfur (S) attracts particular interests due to its high specific capacity of 1,675 $mAhg^{-1}$ and high energy density of 2,600 $Whkg^{-1}$, which is 10 times higher energy density than that of classical commercial $LiCoO_2$ cathode.[18-24] Furthermore, S is cheap, abundant and environmentally benign.[25-32] However, the practical application of Li–S battery has been prevented by problems arising from insulating nature of S, high solubility and shuttle phenomena of polysulfides, which cause low Coulombic efficiency, less active material utilization and poor cycle life.[22, 32-41] Various strategies have been employed to address these issues, such as optimizing the electrolyte,[35, 42-46] constructing interface,[47] synthesizing composite electrode of S/polymer,[21, 23, 30, 31, 33] S/carbon,[34, 37, 40, 45, 48, 49] S/metal organic framework (MOF)[50] and fabricating oxygenated porous architectures.[13, 22, 32]

Among these strategies, combination of meso/microporous carbon with S has been demonstrated as one of the most effective approaches to increase the active-sulfur utilization, cycle stability and high-rate capability of sulfur cathodes, because the porous carbon possess excellent conductivity, inherently large surface area, and strong meso/microporous adsorption capability as a conductive matrix.[51-53] Recently, Guo et al. reported that confine S_{2-4} in a microporous carbon host with pore size of ~0.5nm could avoid the unfavorable transition between S_8 and S_4^{2-}, leading to improved cyclability and rate capability.[54] Therefore, by deliberately creating porosity and controlling pore size of the carbon host, sufficient space for sulfur storage as well as electrolyte pathways is guaranteed. [20, 36, 54]

However, most of the reported carbon/S composites as electrode materials have required the use of carbon black additives and polymer binders to assure mechanical stability and electrical connectivity of the whole system. The introduction of carbon black additives and binders to electrode will definitely result in the lower overall energy density of battery.[30] In addition, the interfaces between active material (carbon-S), binder, and carbon black act as scattering centers for electron transport

View Article Online
DOI: 10.1039/C4NR02498B

resulting in enhanced internal resistances of electrode.[55] To construct a better Li-S battery with high volumetric energy and power density, the most elegant strategy is to design flexible freestanding and binder-free electrode, in which all the materials could participate in lithium storage.[56] Recently, flexible and free-standing carbon/S composites have been reported as high performance cathodes for Li-S battery.[55, 57-61] Huang et al. reported the template-directed synthesis of sulphur/CNT composite as flexible and free-standing cathode material for Li-S batteries and demonstrated an excellent cycle performance.[59]

Therefore, combination of the above-mentioned two aspects, it is ideal to design flexible and free-standing porous carbon host with optimized pore size for S accommodation that can relieve the dissolving of polysulfide while keeping the overall electrode highly conductive as well as improved overall energy density of battery.

Herein, we report on the design of flexible free-standing Li-S battery cathode based on loading sulfur-into an electrospun derived three-dimensinal (3D) interconnected porous carbon nanofibers (PCNFs)-CNT hybrid via a sulfur infiltration method.[62-64] This design could sufficiently utilize the synergistic effects from the porous carbon nanofibers host with optimized pore size for S accommodation and the high conductivity of the CNTs and PCNFs network with excellent mechanical stability.[65] In addition, 3D interconnected porous structure of the PCNFs-CNT with superior electrical conductivity, interconnected porous nature, and large surface area can facilitate the diffusion and transport of electrons and ions, resulting in improved electrochemical performance. The obtained sulphur/(PCNFs-CNT) composite (denoted as S@PCNFs-CNT) shows high rate capability of 437 $mAhg^{-1}$ at 1 Ag^{-1} and excellent cycling stability of 637 $mAhg^{-1}$ after 100 cycles when used as a cathode in a Li–S battery.

2. Experimental

2.1. Electrospinning of PAN-CNT nanofibers

Firstly, MWCNTs were carboxyl functionalized by refluxing with concentrated

View Article Online
DOI: 10.1039/C4NR02498B

HNO_3 as reported.[66] In a typical process, 0.15 g MWCNTs were dissolved in 9 g N,N-dimethylformamide (DMF, SCRC) and sonicated for half an hour. Next, 0.85 g polyacrylonitrile (PAN, MW=150 000, Aldrich) was dissolved in the above solution to prepare the precursor for electrospinning. The solution was loaded into 10ml syringe with 19-gauge blunt tip and spun by applying a positive voltage of 17 kV. The syringe was pushed by a syringe pump with a feeding rate of 19.00 $\mu lmin^{-1}$. The distance between tip of needle and the rotating cylinder was kept as 20 cm. For comparison, MWCNTs-free PAN nanofibers were prepared at the same condition.

2.2. Formation of porous carbon nanofibers-CNT composite (PCNFs-CNT)

The as-collected electrospun PANs-CNT were stabilized in air at 280 °C for 3 h with a heating rate of 2 $Kmin^{-1}$. Subsequently, the above stabilized fibers were carbonized at 800 °C for 5 h with a heating rate of 5 $Kmin^{-1}$ to prepare CNFs-CNT. The obtained CNFs-CNT (0.05 g) and KOH (0.5 g) (CNFs-CNT: KOH=1:10, weight ratio) were added into 20 ml deionized water and then the mixture was stirred for 12 h. The mixture product was filtered and dried at 80 °C in an oven. After that the CNFs-CNT was chemical active at 800 °C with a heating rate of 5 °C min^{-1} for 0.5 h under Ar. Following, CNFs-CNT was washed with deionized water until the pH of filtrate is neutral and dried in an oven at 80 °C. Finally, the result in porous CNF-CNT nanofibers (denoted as PCNFs-CNT) was obtained. For comparison, the CNT-free porous CNFs was also prepared under the same procedure.

2.3. Preparation of flexible free-standing S@PCNFs-CNT

The obtained PCNFs-CNT was tailored into several small pieces (1.5 cm × 1.5 cm). Then mixture of sulfur and PCNFs-CNT paper in the weight ratio of 1:1 were co-heated at 155 °C for 8 h in an autoclave under argon atmosphere to get S@PCNFs-CNT. For comparison, sulfur infiltrating porous CNFs (denoted as S@PCNFs) was also fabricated via a similar treatment.

2.4. Structural analysis and electrochemical measurements

X-ray powder diffraction (XRD) (Philips X'Pert PRO SUPER X-ray diffractometer with Cu-Kα radiation) was employed to characterize the structural properties of the samples. The morphologies of the samples were characterized by Filed-Emission

View Article Online
DOI: 10.1039/C4NR02498B

Scanning electron microscopy (FESEM, JEOL, Tokyo, Japan), transmission electron microscopy (TEM, JEOL, Tokyo, Japan) and high-resolution TEM (HRTEM). The Raman spectroscopy was used to study the degree of graphitization. An ASAP 2020 Accelerated Surface Area and Porosimetry instrument was used to measure the products' nitrogen adsorption/desorption isotherms. Thermogravimetry (TG) was involved in determining the sulfur contents in the S@PCNFs-CNT and S@PCNFs. The mechanical property of S@PCNFs-CNT and S@PCNFs were tested using DMA 800 at room temperature from 0 to 15 N at a rate of 0.0500 $Nmin^{-1}$.

The free-standing S@PCNFs-CNT (or S@PCNFs) was directly used as the working electrode to perform batteries with 2032 coin cells with Li metal as counter and reference electrodes. The areal sulfur loading in the Li-S cell electrode is about 0.8 mg/cm^2. The electrolyte consists of 1 M $LiPF_6$ in ethylene carbonate -dimethyl carbonate (W_{EC}:W_{DMC}=1:1, Guotai Huarong New Chemical materials Co., Ltd). Glass fiber (Whatman) was used as a separator film. The cells were assembled in an argon-filled glove box (MBRAUN LABMASTER 130) where both moisture and oxygen levels were kept below 1ppm. The galvanostatic charge-discharge tests were carried out at a voltage window of 1.00-3.00 V on a battery test system (Neware BTS-610). The specific capacity was calculated on the basis of the active sulfur material. Cyclic voltammetry measurements were conducted at a scan rate of 0.2 mVs^{-1}. Electrochemical impedance spectrum (EIS) measurements were performed on a CHI 660D electrochemical workstation (Chenhua Instrument Company, Shanghai, China) in the frequency range from 100 kHz to 0.01 Hz.

3. Results and discussion

3.1 Structural and Morphological Characterization

The fabrication procedure of S@PCNFs-CNT was illustrated in Figure 1. Firstly, the mixture of PAN-CNT/DMF was electrospun into fibers by electrospinning technique (Fig. 1A). As shown in Fig. 1B, the as-collected PAN-CNT fibers were stabilized in air at 280 °C, followed by carbonization in Ar at 800 °C to get CNFs-CNT composite. The obtained CNFs-CNT was subsequently chemically

View Article Online
DOI: 10.1039/C4NR02498B

activated with KOH in Ar atmosphere, resulting in PCNFs-CNT. Finally, after heating of the mixture of S and PCNFs-CNT, sulfur diffuses into the pores of PCNFs-CNT to form the sulphur/(PCNFs-CNT) composite (S@PCNFs-CNT). For comparison, sulfur loading in CNT-free PCNFs (S@PCNFs) was prepared using a similar process. The obtained sulfur/carbon composites (S@PCNFs-CNT or S@PCNFs) were directly cut and then tested as flexible free-standing cathode material for Li-S batteries (Fig. 1C and D).

Field-emission scanning electron microscopy (FESEM) images of electrospun PAN-CNT (Figure 2A) nanofibers and PAN nanofibers (Figure 2B) exhibit similar long and straight fibrous morphology. The diameter of PAN (Figure 2B) fibers was about 400 nm. In case of the PAN-CNT (Figure 2A), it shows smaller diameter than that of PAN, which is ascribed to the addition of CNTs. This is consistent with previous reports.[65] After carbonization and activation, the morphologies of PCNFs-CNT (Figure 2C) fibers and PCNFs fibers (Figure 2D) change from straight to undulated fibers are caused by a large weight loss accompanied with gas evolution (e.g., CO, CO_2, H_2O, etc).[56] As a result, the average diameters of PCNFs-CNT and PCNFs decrease to 100 and 250 nm, respectively. After S infiltration into PCNFs-CNT and PCNFs, there was no large change in macromorphology (Fig. 2E & 2F). And no sulfur residues can be observed on the surfaces of both nanofibers.

The microstructure of S@PCNFs-CNT and S@PCNFs was further investigated by transmission electron microscopy (TEM). Figure 3A clearly show CNT encapsulated in PCNFs. The diameter of S@PCNFs-CNT and CNT is about 130 and 30 nm, respectively. The HRTEM image in Fig. 3B shows some graphite layers with a spacing of 0.34 nm embedded in PCNFs, that is confirmed by selected area electron diffraction (SAED) image (inset of Fig.3B). The S@PCNFs shows a diameter about 250 nm (Fig. 3C). The HRTEM image of S@PCNFs (Fig. 3D) reveals the formation of randomly oriented crystallites that is in good agreement with SAED image (inset of Fig.3D).

Figure 4 shows Raman spectra of S@PCNFs-CNT and S@PCNFs composite nanofibers. Both samples show well-known D-band (disorder-induced phonon mode)

View Article Online
DOI: 10.1039/C4NR02498B

at about 1350 cm^{-1} and G-band (graphite band) at about 1580 cm^{-1}. The ratio (R) of the intensity of D-band and G-band is a reflection of the degree of graphitization and the alignment of graphitic planes. The R value of S@PCNFs-CNT can be calculated as 0.976, smaller than that of S@PCNFs (R=0.990), indicating the presence of more ordered carbon in PCNFs-CNT hybrid.[65]

The specific surface area analysis was performed by nitrogen Brunauer-Emmett-Teller (BET) adsorption measurements. Fig. 5A and B show the BET and pore size distribution of PCNFs-CNT, PCNFs and S@PCNFs-CNT. The porosity of CNFs-CNT obtained by N_2 adsorption analysis indicates a low specific surface area of 217 m^2g^{-1}, and a pore size of micropores (peaked at 0.5 nm). After activation, the BET surface area of PCNFs-CNT increases to 803 m^2g^{-1}, and PCNFs-CNT posses both mesopores (peaked at 2.5 nm) and micropores (peaked at 0.5 nm and 1.4 nm). The unique microporous structure of PCNFs-CNT can easily accommodate short chains of S in the low-molecular forms for the sulfur.[40, 54] After sulfurizing, the BET surface area of S@PCNFs-CNT sharply reduces to 148 m^2g^{-1}, accompanied by a disappearance of the micropores. It proves that sulfur is infiltrated to the micropores of PCNFs-CNT and the main sulfur existence would like to be chain-like sulfur molecules.[67] For the activation process and sulfurizing process of CNFs, similar phenomenon is observed from the BET and pore size distribution results (Fig. 5C and D), indicating the filtration of sulfur into the pore of PCNFs.

Scanning transmission electron microscopy (STEM) image of S@PCNFs-CNT in Fig. 6A displays a smooth surface, suggesting the S accommodation in the carbon nanofibers uniformly. In addition, elemental mapping of S (Fig. 6B) and Carbon (Fig. 6C) reveal a uniform distribution of sulfur in the PCNFs-CNT. The absence of all characteristic peaks of α-S_8 in the XRD patterns of both samples indicate a fine dispersion of sulfur into PCNFs-CNT and PCNFs (Fig. 6D), respectively. Thermogravimetry (TG) analyses of the S@PCNFs-CNT and S@PCNFs confirm that the sulfur contents of the two samples is 40% and 39%, respectively (Fig. 6E&F).

3.2 Electrochemical performance

View Article Online
DOI: 10.1039/C4NR02498B

Fig. 7 shows cyclic voltammetry (CV) curves of the S@PCNFs-CNT and S@PCNFs cycled in the potential range of 1.00-3.00 V. For S@PCNFs-CNT (Fig. 7A), there are two main cathodic peaks near 2.3 and 1.4 V in the 1st cycle, corresponding to the change from sulfur to lithium polysulfides and the further reduction of higher-order lithium polysulfides. The cathodic peak at 2.3 V (vs. Li^+/Li) disappears completely after the first cycle because of the dissolution of trace amount of cyclo-S_8 on the surface of carbon nanofibers in electrolyte, indicating that sulfur is almost loaded inside the micropores of PCNFs-CNT.[36, 53, 67] After the 1st cycle, the CV curves are overlapped, suggesting a good electrochemical stability of the chain-like sulfur molecules. In case of S@PCNFs (Fig. 7B), the cathodic and anodic peaks after the 1st cycle are at 1.25 V and 2.4 V (vs. Li^+/Li),respectively, indicating a higher polarization of S@PCNFs than that of S@PCNFs-CNT during cycling.

Figure 8A and B show the charge/discharge profiles of the S@PCNFs-CNT and S@PCNFs electrodes from the 1st to the 3rd cycle at a current density of 0.05 A g^{-1} in the voltage window of 1.00-3.00 V, respectively. For the 1st discharge process of S@PCNFs-CNT (Fig. 8A), there are two potential plateaus at about 2.4 V and 1.8 V (vs. Li^+/Li), respectively, corresponding to the two-step reaction of sulfur with lithium. [27, 67] The voltage slope between 1.5 and 1.0 V results from the interaction between sulfur and carbon.[68] Only one plateau (~ 2.1 V) is observed in the initial charge process, which relates to the delithiation of chain-like sulfur molecules. The initial discharge and charge capacities of S@PCNFs-CNT are 1,592 mAh g^{-1} and 860 $mAhg^{-1}$, respectively, indicating an initial Coulombic efficiency (CE) of 53.9%.[67] The plateau of the 1st discharge process at 2.4 V disappears after the first cycle, which is consistent with the CV curves. There is only one discharge potential plateau of about 1.8 V after the 1st cycle, which is mainly attributed to strong absorbability resulting from the formation of some special complexes with carbon or surface-bonded oxygen for active carbon after sulfur embedded in the fine pores of PCNFs-CNT.[69] In case of the S@PCNFs (Fig. 8B), the initial discharge and charge capacities are 1,226 $mAhg^{-1}$ and 383 $mAhg^{-1}$, respectively, corresponding to the initial CE of 31.2%. The large irreversible capacity loss of both samples are caused by the

View Article Online
DOI: 10.1039/C4NR02498B

irreversible reaction of lithium with the porous carbon matrix which has a large surface area and the reaction between cyclo-S_8 and carbonate solvents in the first discharge process.[13, 54]

Figure 8C compares the cycle performance of S@PCNFs-CNT and S@PCNFs electrodes at current density of 0.05 Ag^{-1}. The S@PCNFs-CNT electrode retains a reversible capacity of 637 $mAhg^{-1}$, much higher than those of the S@PCNFs (334 $mAhg^{-1}$) after 100 cycles. After the initial cycle, the CE of both samples reaches ~100%, indicating effectively host effect of S@PCNFs-CNT and S@PCNFs to trap dissolved active materials and inhibit their shuttle phenomena. The rate capabilities of the both electrodes were investigated (Fig. 8D). The flexible free-standing S@PCNFs-CNT also exhibits an enhanced high-rate capability. It delivers a reversible capacity as high as 645, 575, 500, and 437 $mAhg^{-1}$ when cycled at a current density of 0.1, 0.2, 0.5, and 1 Ag^{-1}, respectively. When the current density was tuned back to 50 mAg^{-1}, the reversible capacity recovers to 588 $mAhg^{-1}$, suggesting an excellent cycling stability of the electrode. Such cycle performance and rate capability are comparable with previous works on carbon-based Li-S cathodes with carbon black additives and polymer binders.[40, 70] While for S@PCNFs electrode, it only exhibits much worse rate capability (144 $mAhg^{-1}$ at $1Ag^{-1}$). The enhanced capacity of S@PCNFs-CNT electrode (especially at high rates) is attributed to its unique microporous structure of PCNFs-CNT hybrid nanofibers as conductive matrix. The micropores facilitate cycle life by effectively confining polysulfide anion diffusion in the organic electrolyte.[71] In addition, the excellent electrical conductivity provided by the sp^2-hybridized nanocarbon (CNT) and interconnected 3D network of the electrode guarantee rapid electron/ion transport at the PCNFs-CNT/electrolyte interfaces.[36, 71, 72]

To get insight into the interface charge-transfer resistance, S@PCNFs-CNT and S@PCNFs electrodes (discharged to 1.08 V after 18 cycles at 0.2 C) were analyzed using electrochemical impedance spectroscopy (EIS) (Fig. 9A). For both samples, the spectra consist of two depressed semicircles in the high- and middle- frequency regions and a straight line in the low-frequency region. The semicircle in the low

View Article Online
DOI: 10.1039/C4NR02498B

frequency region is related to the interface charge-transfer process of the electrode caused by the formation of an insulating layer of Li_2S.[73] The charge-transfer resistance (R_{ct}) of S@PCNFs-CNT simulated from the equivalent circuits is much smaller than that of S@PCNFs, which is ascribed to the formation of less insulating layer of Li_2S on the surface of S@PCNFs-CNT. Therefore, sulfur is almost loaded inside the micropores of PCNFs-CNT and the electrochemical reaction process confined inside the micropores of PCNFs-CNT.[53]

After cycled for 100 cycles at a current density of 50 mAg^{-1}, the S@PCNFs-CNT electrode tested in Fig. 6C was disassembled in the fully charged condition. The shape, size and structural integrity of the original S@PCNFs-CNT electrode are well maintained, demonstrating excellent structure stability. SEM of S@PCNFs-CNT electrode after 100 cycles at 50 mAg^{-1} was also investigated. Except that the surface becomes rough, the morphology of S@PCNFs-CNT remains similar diameter with no obvious fracture on the surface (Fig. 9B).

The mechanical property of S@PCNFs-CNT and S@PCNFs are also tested using DMA 800 at room temperature from 0 to 15 N at a rate of 0.0500 $Nmin^{-1}$ (Fig. 10). Samples of S@PCNFs-CNT and S@PCNFs for tensile testing are 8.30 mm*4.20 mm*0.064 mm and 8.96 mm*3.94 mm*0.052 mm, respectively. The strain of the two samples are nearly equal (2.846% S@PCNFs-CNT and 3.034% for S@PCNFs) when the matrixes fracture. The stress of S@PCNFs-CNT is a little lower than S@PCNFs (0.2739 MPa for S@PCNFs-CNT and 0.4700 MPa for S@PCNFs),which may ascribe to the inhomogeneous dispersion of CNT in the PCNFs matrix.[74-76]

The improvement of electrochemical performance of S@PCNFs-CNT can be explained as following. i) The uniform distribution of micropores can provide sufficient host to accommodate sulfur molecule as well as fast migration of Li^+.[40] The chain-like sulfur molecules confined in the micropores can efficiently prevent the generation of electrolyte-soluble polysulfides.[36, 67] ii) The 3D interconnected nanofibers structure can provide short ion transfer length and continuous electron transportation path.[77, 78] iii) The introduction of CNT into PCNFs-CNT can improve

View Article Online
DOI: 10.1039/C4NR02498B

the electronic conductivity of material,[65] which is helpful to the electrochemical activity of Sulfur, especially for rate performance of Li-S batteries.[40]

4. Conclusions

In summary, we have prepared flexible and free-standing sulfur/porous carbon nanofibers-CNT composite (S@PCNFs-CNT) as cathode for Li-S batteries via a two-step method. First, the PCNFs-CNT was fabricated by chemical activation of carbonized electrospun PAN-CNT nanofibers. Second, sulfur infiltration into the micropores of PCNFs-CNT through a co-heating process. When used as a cathode material for Li-S batteries, the S@PCNFs-CNT exhibits an excellent lithium storage performance, enhanced cycle stability and high rate capacity. It delivers a reversible capacity of 637 $mAhg^{-1}$ after 100 cycles at 50 mAg^{-1} and a rate capability of 437 $mAhg^{-1}$ at 1 Ag^{-1}. The improved electrochemical performance is attributed to synergistic effect of the 3D interconnected structure, the additive of CNT, the uniform distribution of micropores (< 2 nm) in the PCNFs-CNT matrix. This design of flexible and free-standing electrode offers an effective technique to boost electrochemical performances of electrode materials, and can be extended to synthesize other cathode (or anode)/PCNFs-CNT hybrid electrodes for Li-ion batteries.

Acknowledgements

This work was financially supported by the National Natural Science Foundation of China (No.21171015, No.21373195), The Recruitment Program of Global Experts, program for New Century Excellent Talents in University (NCET), the Fundamental Research Funds for the Central Universities (WK2060140014, WK2060140016) and sofja kovalevskaja award from Alexander von Humboldt Foundation.

View Article Online
DOI: 10.1039/C4NR02498B

References:

[1] Y. Zhang, L. Wang, A. Zhang, Y. Song, X. Li, H. Feng, X. Wu, P. Du, Solid State Ionics 2010, 181, 835.

[2] Y. Zhang, A. Q. Zhang, Y. H. Gui, L. Z. Wang, X. B. Wu, C. F. Zhang, P. Zhang, Journal of Power Sources 2008, 185, 492.

[3] Y. Zhang, Y. Zhao, K. E. Sun, P. Chen*, The Open Materials Science Journal 2011, 1874.

[4] G. Xu, B. Ding, P. Nie, L. Shen, J. Wang, X. Zhang, Chemistry 2013, 19, 12306.

[5] K. Ozawa, Solid State Ionics 1994, 69, 212.

[6] W. Liu, G. C. Farrington, F. Chaput, B. Dunn, Journal of the Electrochemical Society 1996, 143, 879.

[7] R. Dominko, M. Bele, M. Gaberscek, M. Remskar, D. Hanzel, S. Pejovnik, J. Jamnik, Journal of the Electrochemical Society 2005, 152, A607.

[8] X. Ji, L. F. Nazar, Journal of Materials Chemistry 2010, 20, 9821.

[9] S. Evers, L. F. Nazar, Accounts of Chemical Research 2013, 46, 1135.

[10] A. Manthiram, Y. Fu, Y. S. Su, Accounts of Chemical Research 2013, 46, 1125.

[11] Y. Fu, C. Zu, A. Manthiram, Journal of the American Chemical Society 2013, 135, 18044.

[12] P. G. Bruce, S. A. Freunberger, L. J. Hardwick, J. M. Tarascon, Nature materials 2012, 11, 19.

[13] L. Q. Lu, L. J. Lu, Y. Wang, Journal of Materials Chemistry A 2013, 1, 9173.

[14] W. Li, G. Zheng, Y. Yang, Z. W. Seh, N. Liu, Y. Cui, Proceedings of the National Academy of Sciences of the United States of America 2013, 110, 7148.

[15] S. Zheng, Y. Chen, Y. Xu, F. Yi, Y. Zhu, Y. Liu, J. Yang, C. Wang, ACS nano 2013, 7, 10995.

[16] Z. W. Seh, H. Wang, P.-C. Hsu, Q. Zhang, W. Li, G. Zheng, H. Yao, Y. Cui, Energy & Environmental Science 2014, 7, 672.

[17] Z. W. Seh, H. Wang, N. Liu, G. Zheng, W. Li, H. Yao, Y. Cui, Chemical Science 2014.

[18] G. Zheng, Y. Yang, J. J. Cha, S. S. Hong, Y. Cui, Nano letters 2011, 11, 4462.

[19] G. Zheng, Q. Zhang, J. J. Cha, Y. Yang, W. Li, Z. W. Seh, Y. Cui, Nano letters 2013, 13, 1265.

[20] G. He, S. Evers, X. Liang, M. Cuisinier, A. Garsuch, L. F. Nazar, ACS nano 2013, 7, 10920.

[21] G. Zhou, S. Pei, L. Li, D. W. Wang, S. Wang, K. Huang, L. C. Yin, F. Li, H. M. Cheng, Advanced materials 2014, 26, 625.

[22] L. Ji, M. Rao, H. Zheng, L. Zhang, Y. Li, W. Duan, J. Guo, E. J. Cairns, Y. Zhang, Journal of the American Chemical Society 2011, 133, 18522.

[23] Z. Dong, J. Zhang, X. Zhao, J. Tu, Q. Su, G. Du, RSC Advances 2013, 3, 24914.

[24] S. E. Cheon, K. S. Ko, J. H. Cho, S. W. Kim, E. Y. Chin, H. T. Kim, Journal of the Electrochemical Society 2003, 150, A796.

[25] A. Patil, V. Patil, D. Wook Shin, J. W. Choi, D. S. Paik, S. J. Yoon, Materials Research Bulletin 2008, 43, 1913.

[26] Y.-S. Su, A. Manthiram, Nature Communications 2012, 3, 1166.

[27] Y. V. Mikhaylik, J. R. Akridge, Journal of the Electrochemical Society 2004, 151, A1969.

[28] Y. Yan, Y.-X. Yin, S. Xin, J. Su, Y.-G. Guo, L.-J. Wan, Electrochimica Acta 2013, 91, 58.

[29] J. Guo, Z. Yang, Y. Yu, H. D. Abruña, L. A. Archer, Journal of the American Chemical Society 2013, 135, 763.

[30] H. Wang, Y. Yang, Y. Liang, J. T. Robinson, Y. Li, A. Jackson, Y. Cui, H. Dai, Nano letters 2011, 11, 2644.

[31] X. Liang, Y. Liu, Z. Wen, L. Huang, X. Wang, H. Zhang, Journal of Power Sources 2011, 196,

View Article Online
DOI: 10.1039/C4NR02498B

6951.

[32] J. Fanous, M. Wegner, J. Grimminger, Ä. Andresen, M. R. Buchmeiser, Chemistry of Materials 2011, 23, 5024.

[33] W. Li, Q. Zhang, G. Zheng, Z. W. Seh, H. Yao, Y. Cui, Nano letters 2013, 13, 5534.

[34] X. Ji, K. T. Lee, L. F. Nazar, Nature materials 2009, 8, 500.

[35] J. Wang, Z. Yao, C. W. Monroe, J. Yang, Y. Nuli, Advanced Functional Materials 2013, 23, 1194.

[36] S. Xin, L. Gu, N. H. Zhao, Y. X. Yin, L. J. Zhou, Y. G. Guo, L. J. Wan, Journal of the American Chemical Society 2012, 134, 18510.

[37] J. Wang, L. Yin, H. Jia, H. Yu, Y. He, J. Yang, C. W. Monroe, ChemSusChem 2014, 7, 563.

[38] M. Cuisinier, P.-E. Cabelguen, S. Evers, G. He, M. Kolbeck, A. Garsuch, T. Bolin, M. Balasubramanian, L. F. Nazar, The Journal of Physical Chemistry Letters 2013, 4, 3227.

[39] Y. S. Su, Y. Fu, B. Guo, S. Dai, A. Manthiram, Chemistry 2013, 19, 8621.

[40] J. T. Lee, Y. Zhao, S. Thieme, H. Kim, M. Oschatz, L. Borchardt, A. Magasinski, W. I. Cho, S. Kaskel, G. Yushin, Advanced materials 2013, 25, 4573.

[41] Y. Yang, G. Zheng, S. Misra, J. Nelson, M. F. Toney, Y. Cui, Journal of the American Chemical Society 2012, 134, 15387.

[42] D. Aurbach, E. Pollak, R. Elazari, G. Salitra, C. S. Kelley, J. Affinito, Journal of The Electrochemical Society 2009, 156, A694.

[43] Y. Yang, G. Zheng, Y. Cui, Energy & Environmental Science 2013, 6, 1552.

[44] Z. W. Seh, Q. Zhang, W. Li, G. Zheng, H. Yao, Y. Cui, Chemical Science 2013, 4, 3673.

[45] X. Ji, S. Evers, R. Black, L. F. Nazar, Nat Commun 2011, 2, 325.

[46] C. Huang, J. Xiao, Y. Shao, J. Zheng, W. D. Bennett, D. Lu, S. V. Laxmikant, M. Engelhard, L. Ji, J. Zhang, X. Li, G. L. Graff, J. Liu, Nature Communications 2014, 5.

[47] L. Wang, D. Wang, F. Zhang, J. Jin, Nano letters 2013, 13, 4206.

[48] N. Jayaprakash, J. Shen, S. S. Moganty, A. Corona, L. A. Archer, Angewandte Chemie - International Edition 2011, 50, 5904.

[49] R. Elazari, G. Salitra, A. Garsuch, A. Panchenko, D. Aurbach, Advanced materials 2011, 23, 5641.

[50] K. Xi, S. Cao, X. Y. Peng, C. Ducati, R. V. Kumar, A. K. Cheetham, Chemical Communications 2013, 49, 2192.

[51] C. Lai, X. P. Gao, B. Zhang, T. Y. Yan, Z. Zhou, Journal of Physical Chemistry C 2009, 113, 4712.

[52] B. Zhang, C. Lai, Z. Zhou, X. P. Gao, Electrochimica Acta 2009, 54, 3708.

[53] B. Zhang, X. Qin, G. R. Li, X. P. Gao, Energy & Environmental Science 2010, 3, 1531.

[54] H. Ye, Y.-X. Yin, S. Xin, Y.-G. Guo, Journal of Materials Chemistry A 2013, 1, 6602.

[55] K. Xi, P. R. Kidambi, R. Chen, C. Gao, X. Peng, C. Ducati, S. Hofmann, R. V. Kumar, Nanoscale 2014.

[56] W. Li, L. Zeng, Z. Yang, L. Gu, J. Wang, X. Liu, J. Cheng, Y. Yu, Nanoscale 2014, 6, 693.

[57] J. Jin, Z. Wen, G. Ma, Y. Lu, Y. Cui, M. Wu, X. Liang, X. Wu, RSC Advances 2013, 3, 2558.

[58] G. M. Zhou, L. C. Yin, D. W. Wang, L. Li, S. F. Pei, I. R. Gentle, F. Li, H. M. Cheng, ACS nano 2013, 7, 5367.

[59] G. Zhou, D.-W. Wang, F. Li, P.-X. Hou, L. Yin, C. Liu, G. Q. Lu, I. R. Gentle, H.-M. Cheng, Energy & Environmental Science 2012, 5, 8901.

[60] J.-Q. Huang, H.-J. Peng, X.-Y. Liu, J.-Q. Nie, X.-B. Cheng, Q. Zhang, F. Wei, Journal of Materials Chemistry A 2014.

[61] K. Jin, X. Zhou, L. Zhang, X. Xin, G. Wang, Z. Liu, The Journal of Physical Chemistry C 2013,

View Article Online
DOI: 10.1039/C4NR02498B

117, 21112.
[62] M. Inagaki, Y. Yang, F. Kang, Advanced materials 2012, 24, 2547.
[63] Y. Yu, L. Gu, C. Wang, A. Dhanabalan, P. A. van Aken, J. Maier, Angewandte Chemie 2009, 48, 6485.
[64] Y. Yu, L. Gu, C. B. Zhu, P. A. van Aken, J. Maier, Journal of the American Chemical Society 2009, 131, 15984.
[65] T. Maitra, S. Sharma, A. Srivastava, Y.-K. Cho, M. Madou, A. Sharma, Carbon 2012, 50, 1753.
[66] Z. Peining, A. S. Nair, Y. Shengyuan, S. Ramakrishna, Materials Research Bulletin 2011, 46, 588.
[67] S. Xin, Y.-X. Yin, L.-J. Wan, Y.-G. Guo, Particle & Particle Systems Characterization 2013, 30, 321.
[68] D. W. Wang, G. Zhou, F. Li, K. H. Wu, G. Q. Lu, H. M. Cheng, I. R. Gentle, Physical chemistry chemical physics : PCCP 2012.
[69] J. L. Wang, J. Yang, J. Y. Xie, N. X. Xu, Y. Li, Electrochemistry Communications 2002, 4, 499.
[70] J. Yang, J. Xie, X. Zhou, Y. Zou, J. Tang, S. Wang, F. Chen, L. Wang, The Journal of Physical Chemistry C 2014, 118, 1800.
[71] H.-J. Peng, J.-Q. Huang, M.-Q. Zhao, Q. Zhang, X.-B. Cheng, X.-Y. Liu, W.-Z. Qian, F. Wei, Advanced Functional Materials 2014, 24, 2772.
[72] Z. Xiao, Z. Yang, H. Nie, Y. Lu, K. Yang, S. Huang, Journal of Materials Chemistry A 2014, 2, 8683.
[73] J. Shim, K. A. Striebel, E. J. Cairns, Journal of The Electrochemical Society 2002, 149, A1321.
[74] H. Lee, S. Mall, P. He, D. Shi, S. Narasimhadevara, Y.-H. Yun, V. Shanov, M. J. Schulz, Composites Part B: Engineering 2007, 38, 58.
[75] D. Shi, J. Lian, P. He, L. M. Wang, F. Xiao, L. Yang, M. J. Schulz, D. B. Mast, Applied Physics Letters 2003, 83, 5301.
[76] E. T. Thostenson, Z. F. Ren, T. W. Chou, Composites Science and Technology 2001, 61, 1899.
[77] K. Tang, Y. Yu, X. Mu, P. A. van Aken, J. Maier, Electrochemistry Communications 2013, 28, 54.
[78] K. Tang, X. K. Mu, P. A. van Aken, Y. Yu, J. Maier, Advanced Energy Materials 2013, 3, 49.

View Article Online
DOI: 10.1039/C4NR02498B

Figure Captions

Fig. 1 A~B Schematic illustration of the synthesis process for S@PCNFs-CNT electrode.
Fig. 1 C~D Photograph of free-standing and flexible PCNFs electrode.

Fig. 2 FESEM micrographs of as electrospun PAN-CNT nanofibers (A), PAN nanofibers (B), PCNFs-CNT (C), PCNFs (D), S@PCNFs-CNT (E) and S@PCNFs (F). The inset pictures are corresponding high magnification images.

Fig. 3 TEM (A) and HRTEM (B) images of S@PCNFs-CNT. TEM (C) and HRTEM (D) images of S@PCNFs. The inset pictures of (B) and (D) are Selected area electron diffraction (SAED) images of S@PCNFs-CNT and S@PCNFs, respectively.

Fig. 4 Raman patterns of S@PCNFs-CNT and S@PCNFs.

Fig. 5 N_2 sorption/desorption isotherms (A) and pore-size distributions curve (B) of CNFs-CNT, PCNFs-CNT and S@PCNFs-CNT. N_2 sorption/desorption isotherms (C) and pore-size distributions curve (D) of CNFs, PCNFs and S@PCNFs. The pore size distribution was calculated from the adsorption curve using the DFT method.

Fig. 6 Images of Scanning Transmission Electron Microscope (STEM) (A) and corresponding element mapping (sulfur (B), carbon (C)) of one part of an individual S@PCNFs-CNT. (D) XRD patterns of S@PCNFs-CNT and S@PCNFs. Thermogravimetry patterns of S@PCNFs-CNT (E) and S@PCNFs (F).

Fig. 7 Cyclic voltammograms of S@PCNFs-CNT (A) and S@PCNFs (B) electrode between 1 and 3 V at a potential sweep rate of 1 mVs^{-1}.

Fig. 8 Voltage profiles of S@PCNFs-CNT (A) and S@PCNFs (B) electrodes at a current density of 50 mAg^{-1}. (C) Charge capacity-cycle number of S@PCNFs-CNT and S@PCNFs electrodes at a current density of 50 mAg^{-1}.(D) Capacities of

View Article Online
DOI: 10.1039/C4NR02498B

S@PCNFs-CNT and S@PCNFs electrodes as a function of charge− discharge cycles at different charge-discharge current densities of 0.05, 0.1, 0.25, 0.5, 1 Ahg^{-1}, respectively.

Fig. 9 (A) AC impedance spectra of S@PCNFs-CNT/Li cells and S@PCNFs/Li cells after 18 cycles with the equivalent circuit as the inset. The open-circuit-voltage of electrode was controlled similarly (~ 1.08 V), and the weight of electrode was 0.48 mg. (B) FESEM micrographs of S@PCNFs-CNT after 100 cycles between 1.0 V and 3.0 V at a cycling rate of 50 mAg^{-1}. The inset picture is corresponding high magnification image.

Fig. 10 Stress-Strain curve of S@PCNFs-CNT and S@PCNFs from tensile test.

View Article Online
DOI: 10.1039/C4NR02498B

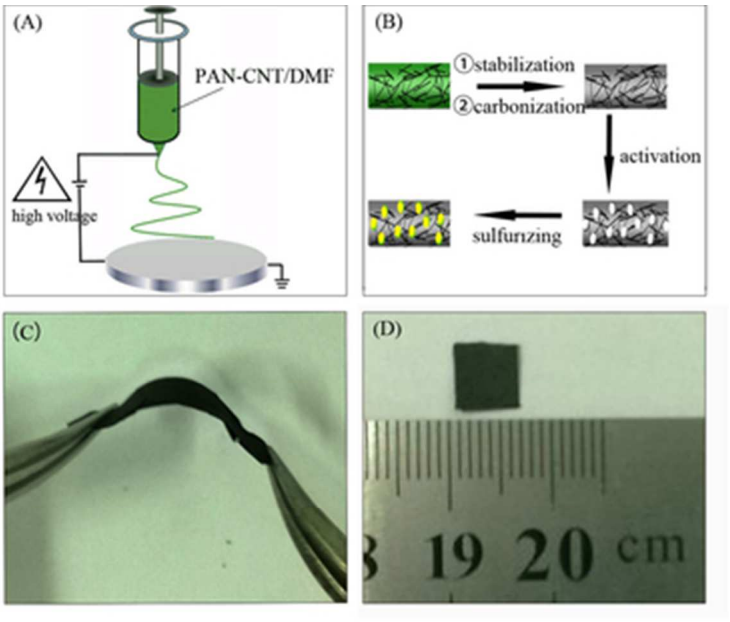

32x26mm (300 x 300 DPI)

View Article Online
DOI: 10.1039/C4NR02498B

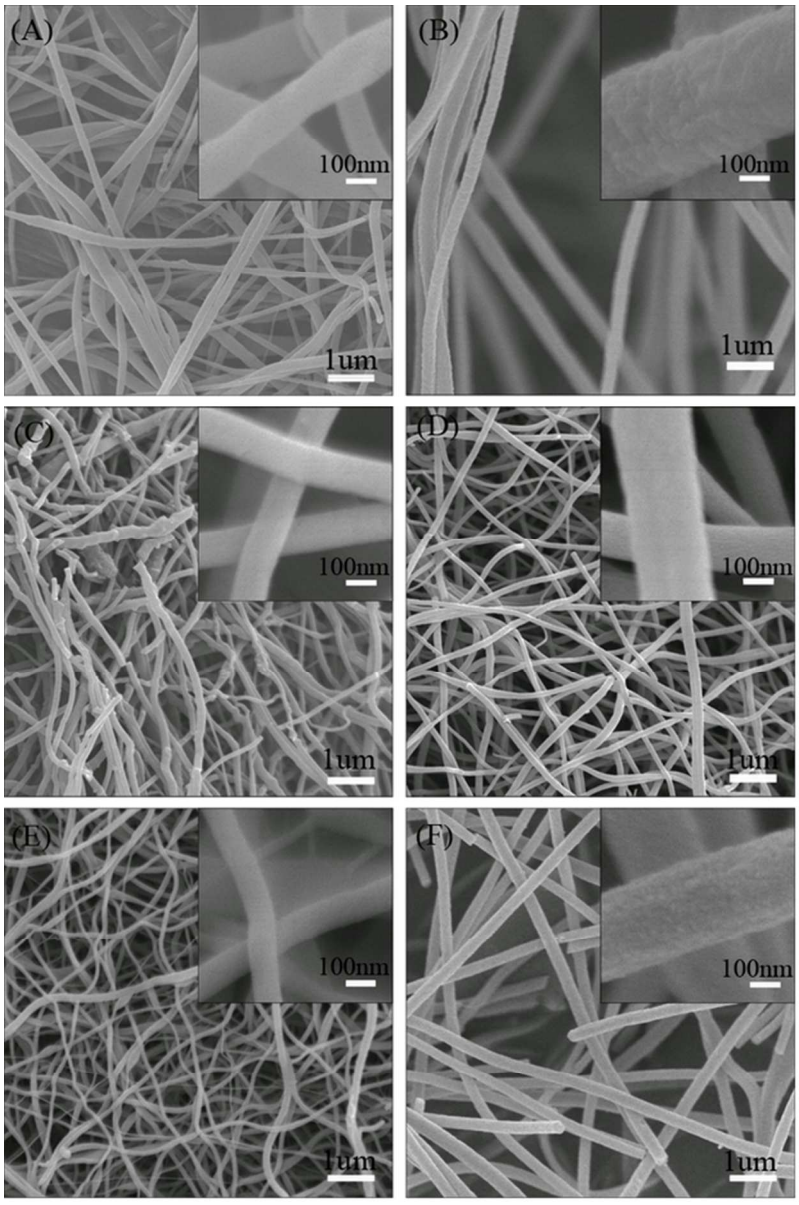

52x78mm (300 x 300 DPI)

View Article Online
DOI: 10.1039/C4NR02498B

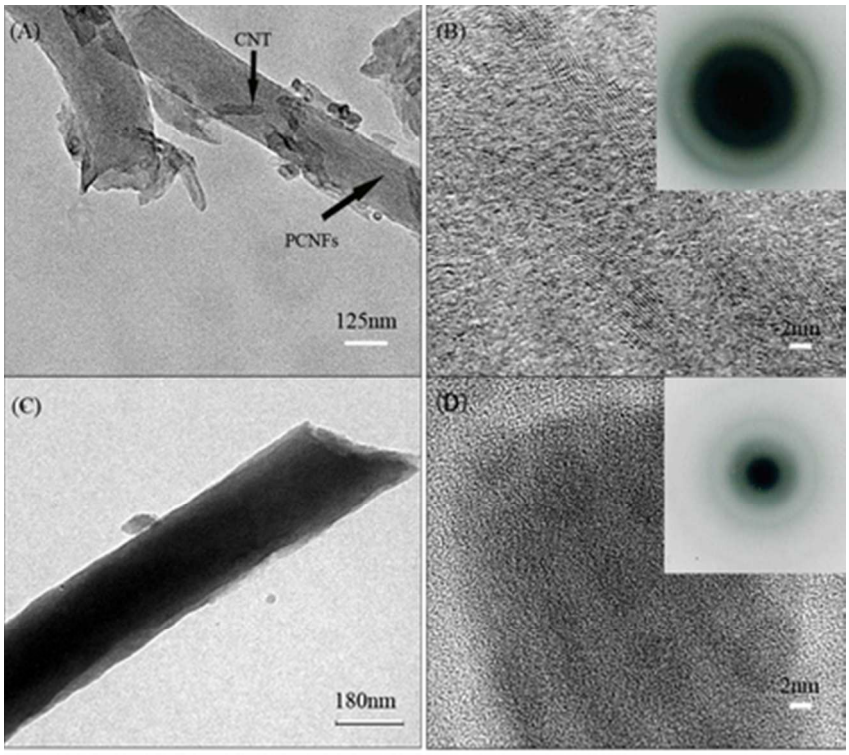

35x31mm (300 x 300 DPI)

View Article Online
DOI: 10.1039/C4NR02498B

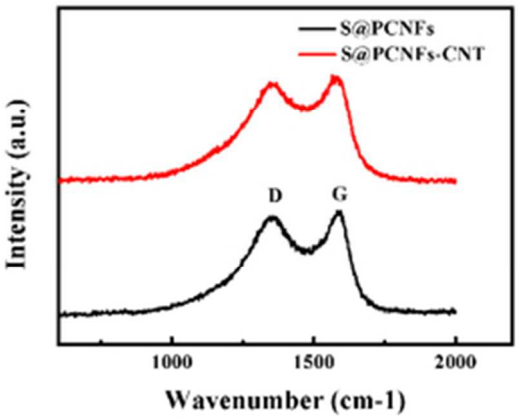

28x19mm (300 x 300 DPI)

View Article Online
DOI: 10.1039/C4NR02498B

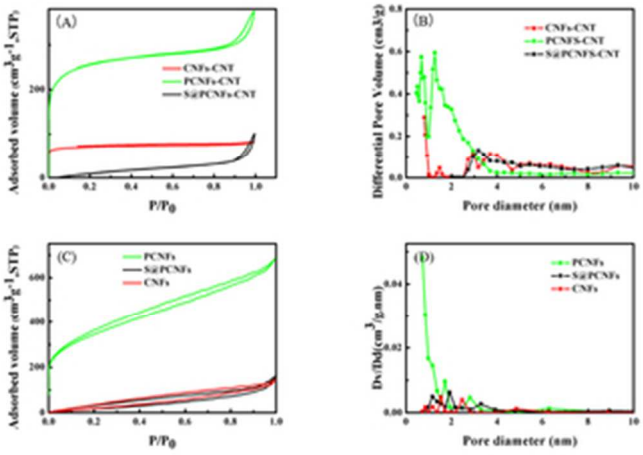

28x20mm (300 x 300 DPI)

View Article Online
DOI: 10.1039/C4NR02498B

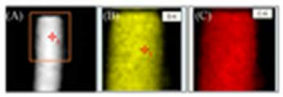

12x3mm (300 x 300 DPI)

View Article Online
DOI: 10.1039/C4NR02498B

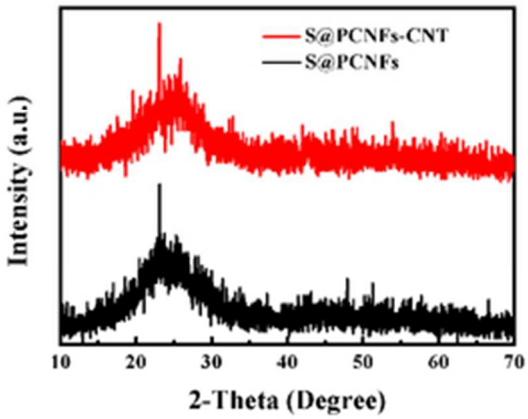

28x19mm (300 x 300 DPI)

View Article Online
DOI: 10.1039/C4NR02498B

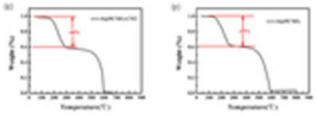

13x4mm (300 x 300 DPI)

View Article Online
DOI: 10.1039/C4NR02498B

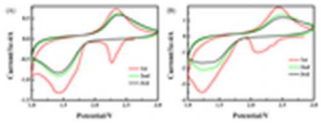

14x4mm (300 x 300 DPI)

View Article Online
DOI: 10.1039/C4NR02498B

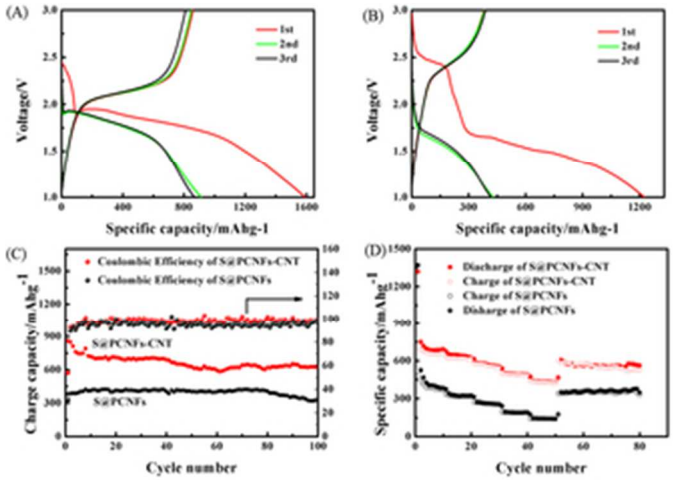

28x20mm (300 x 300 DPI)

View Article Online
DOI: 10.1039/C4NR02498B

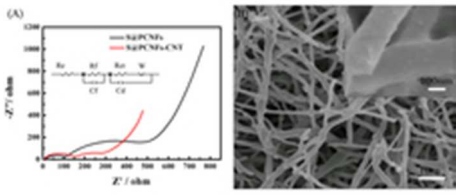

19x9mm (300 x 300 DPI)

View Article Online
DOI: 10.1039/C4NR02498B

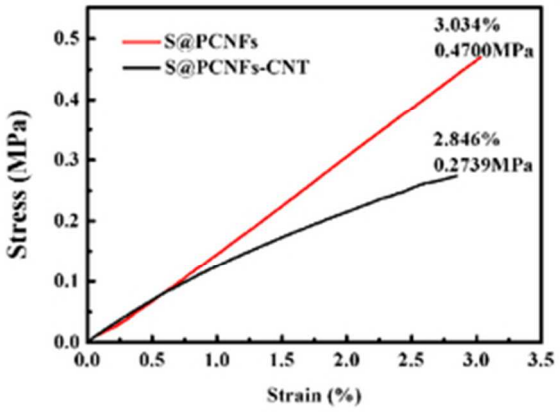

28x19mm (300 x 300 DPI)